Two-dimensional system of hard ellipses: A molecular dynamics study

M. Ebrahim Foulaadvand[1,2,*] and Mohsen Yarifard[1]

[1]*Department of Physics, University of Zanjan, P.O. Box 45196-311, Zanjan, Iran*

[2]*Computational Physical Sciences Research Laboratory, Department of Nano-Sciences, Institute for Research in Fundamental Sciences (IPM), P.O. Box 19395-5531, Tehran, Iran*

(Received 21 March 2013; published 22 November 2013)

We have simulated the dynamics of a two-dimensional system of hard ellipses by event-oriented molecular dynamics in microcanonical NVE ensemble. Various quantities, namely longitudinal and transverse velocity autocorrelation functions, translational and rotational diffusion mean-squared displacements, pressure, intermediate self-scattering function, radial distribution function, and angular spatial correlation, have been obtained and their dependence on packing fraction is characterized. Despite absence of prominent positional ordering, the orientational degree of freedom behaves nontrivially and exhibits interesting features. Slowing down is observed in the angular part of the motion near isotropic-nematic phase transition. It is shown that above a certain packing fraction the rotational mean-squared displacement exhibits a three-stage temporal regime including a plateau. Comparison to 2D system of hard needles is made and it is shown that from positional viewpoint, the ellipse system is more ordered.

DOI: 10.1103/PhysRevE.88.052504 PACS number(s): 61.30.−v, 61.25.Em, 61.20.Ja, 64.70.pp

I. INTRODUCTION

Molecular dynamics (MD) simulation of anisotropic hard objects such as ellipsoids and spherocylinders has been the subject of interest and exploration and has led to much advances in the field of molecular fluids since the pioneering works of Alder and Wainwright [1,2]. For a detailed review, see Ref. [3]. The hard potential is proposed as a simplification of short-range repulsive potential between macro molecules. The proposed model systems have served us as test ground to deepen our understanding on the basic properties of liquids, colloidal suspensions, concentrated polymeric systems, granular systems, and, most importantly, liquid crystalline phases of matter on a molecular level [3–5]. It has been shown that the alignment of nonspherical molecules can lead to a diversity of phases, mainly orientational in nature, in liquid crystals [4,6]. Despite the profound insight obtained via tremendous Monte Carlo (MC) simulations of the static phases [7–9], many dynamical, transportational, and structural properties, namely kinetic arrest and glassy behaviors, have only been poorly understood. In spite of employment of other simulation techniques, like Brownian dynamics [10–12], and theoretical approaches, such as kinetic theory [13,14], density functional [15–17], and hydrodynamics equations approach [18], event-oriented molecular dynamics remains as an efficient tool for probing the dynamical spatial-temporal aspects of hard gases of nonspherical objects. The interplay of positional and orientational degrees of freedom has shown novel aspects in these investigations. Among elongated and anisotropic hard bodies, ellipsoid and ellipses have received quite notable attention [3]. Much progress in our understanding of the behavior of realistic systems can thus be expected from the study of such hardcore model systems. The first simulation attempt, in MC framework, was carried out for a three-dimensional gas of hard ellipsoids by Frenkel and Mulder [19–21]. Shortly afterwards, the first MD simulation was done for a three-dimensional system of hard ellipsoids by Allen and Frenkel [22]. Their simulation confirmed that the isotropic-nematic transition is first order. Further investigations revealed many interesting dynamical properties in hard ellipsoidal systems in 3D such as increase of diffusion coefficient component $D_{\parallel}$ (parallel to director) with density [23] and glassy dynamics [7,8,24,25]. For many practical purposes, we need to know the behavior of a thin film of liquid-crystalline substance. These systems can be effectively considered as 2D. Aside from practical applications, investigation of 2D model systems is interesting from a purely theoretical viewpoint. Villard-Baron did the first pioneering study on a system of ellipses in 2D [26] by MC simulation. The next attempts to study a 2D gas of hard ellipses were theoretical. Boublik [27] implemented the *scaled particle theory*. Ward and Lado numerically solved the Percus-Yevick equation [28]. Cuesta and Tejero implemented density functional approach to describe a 2D system of hard ellipses [29] as a simplified model for the study of mesophases formed by nonspherical molecules absorbed on a smooth surface [30]. Ferreira *et al.* applied hypernetted chain (HNC) equations to the problem [31]. One of the most important findings of Cuesta is that the nature of isotropic-nematic transition is drastically different in 2D and 3D. In a three-dimensional hard ellipsoids system, this transition is first order, while in 2D ellipses gas it is continuous. One year later, Cuesta and Frenkel studied other aspects of the 2D ellipses system via MC simulation [32]. Besides monodisperse hard ellipses system, the properties of its binary fluid mixture has also been investigated [33]. Another interesting system that has been quite extensively studied in 2D and 3D is the needle system [21,34,35]. A needle can be regarded as an extremely elongated ellipse. It has been shown that this simple system exhibits rich behavior [13,36–43]. To the best of our knowledge, MD simulation of a 2D system of ellipses is still lacking in the literature. It allows us to study dynamical properties that cannot be investigated by the mentioned techniques, especially MC simulations. Moreover, our study illuminates the geometrical and entropical features of 2D anisotropic hard systems and provides us with a deeper understanding on the interplay of translational and rotational degrees of freedom in these systems [44].

*foolad@iasbs.ac.ir

II. DESCRIPTION OF THE PROBLEM

Consider a system comprising hard ellipses with mass m, major axis length $2a$, and minor axis length $2b$, which are restricted to move in a two-dimensional x-y plane. The aspect ratio of an ellipse is defined as $\kappa = \frac{a}{b}$. In this paper, we consider only $\kappa = 2$. The interaction between ellipses is assumed to be hardcore; i.e., it is nonzero only when two ellipses are in contact. For simplicity, we work in reduced units such that m and a are taken as one. The moment of inertia tensor I of an ellipse is diagonal and we have $I_{xx} = \frac{mb^2}{4}$ $I_{yy} = \frac{ma^2}{4}$ and $I_{zz} = \frac{m(a^2+b^2)}{4}$. Upon a collision between two ellipses, the center of mass (CM) velocity and the angular velocity around the z axis through the CM will change, in general. We assume that collisions are elastic and frictionless, therefore the energy (entirely kinetic) is conserved after a collision. If the coordinates of the collision point are known, one can find the postcollision velocities in terms of precollision ones by employing the conservation laws of energy, linear and angular momenta. This issue is explained, in details, in Appendix A. Moreover, in Appendix B we discuss how to find the coordinates of the collision point, provided the configuration and velocities of two separate ellipses are given. Determination of the postcollision quantities in terms of the precollision ones enables us to study the dynamics of this 2D ellipse gas within collision-oriented molecular dynamics framework. This approach was first utilized by Alder and Wainwright in the late 1950s to study the dynamic properties of liquids [1,2]. In the event-oriented MD, the evolution of system takes place from collision to collision. The basic task is to find the time of the next collision. We remark that between impulsive collisions, free flight occurs. For an excellent review on the event-oriented molecular dynamics, see Refs. [45] and [46]. In our 2D problem, the free flight of an ellipse consists of a uniform motion of its center of mass plus a free rotation along the z axis with constant angular velocity ω. When two ellipses collide with each other, we refer to one of them as the *collider* ellipse and to the other one as the *partner*. The letters "c" and "p" refer to collider and partner, respectively. See Fig. 1 for illustration of the collision geometry.

We now turn to the molecular dynamics of this two-dimensional fluid. Crucial to the MD of hard objects is the task of finding the collision time between two separate objects. For simple geometry of objects, such as disk or sphere, it is possible to analytically find the collision time and hence the coordinates of the collision point once the initial positions and the velocities (both translational and angular) of the two separate objects is given [47]. However, this task cannot be fulfilled, in principle, when the shape of objects becomes anisotropic like ellipses. Alternatively, we devise a numerical scheme to find the collision time. This scheme has been originally introduced in Refs. [48–50]. The method is based on finding a geometrical condition for overlapping between objects. By overlap we mean a condition when the distance between objects becomes negative. We define the distance between any two rigid objects A and B as the minimum distance between $\mathbf{x}_A$ and $\mathbf{x}_B$ in which $\mathbf{x}_A$ ($\mathbf{x}_B$) is a point on the surface of object A (B) [7]. For ellipses, the overlap condition is explained in Ref. [26]. Let $\hat{u}_1$ and $\hat{u}_2$ be the unit vectors along

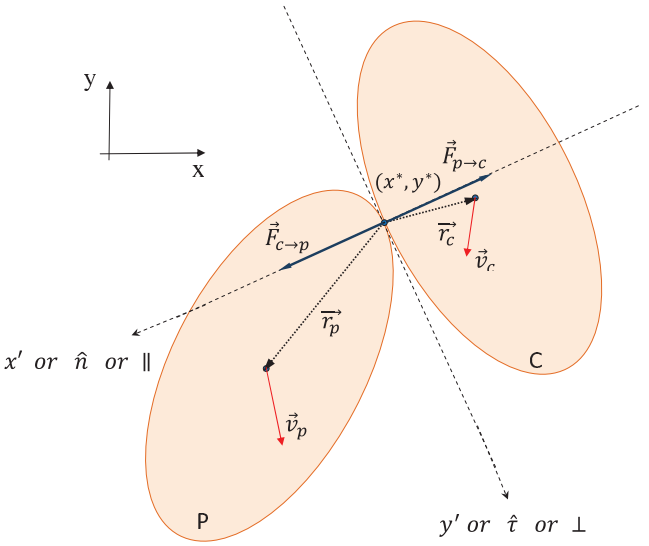

FIG. 1. (Color online) Geometry of an elastic collision between two ellipses. The impulsive forces are exerted along the unit normal vectors at the collision point. The fix frame of reference x-y is shown in the figure.

the major axes of ellipses one and two and $\mathbf{r}$ denotes the vector joining the center of ellipse one to the center of ellipse two. Also, let $\hat{u}_1'$ and $\hat{u}_2'$ denote unit vectors along the perpendicular directions to $\hat{u}_1$ and $\hat{u}_2$, respectively, and θ show the angle between $\hat{u}_1$ and $\hat{u}_2$. Next, a contact function $\Psi(\mathbf{r},\hat{u}_1,\hat{u}_2,a,b)$ is introduced as follows [26]:

$$\Psi = 4\left(f_1^2 - 3f_2\right)\left(f_2^2 - 3f_1\right) - (9 - f_1 f_2)^2, \qquad (1)$$

in which

$$f_\alpha = 1 + G - \left(\frac{\mathbf{r}.\hat{u}_\alpha}{a}\right)^2 - \left(\frac{\mathbf{r}.\hat{u}_\alpha'}{b}\right)^2 \alpha = 1,2, \qquad (2)$$

with $G = 2 + (\frac{a}{b} - \frac{b}{a})^2 \sin^2\theta$. The necessary and sufficient condition for two ellipses to be in contact is that $\Psi = 0$. Moreover, the necessary and sufficient conditions for not having an overlap between ellipses is twofold: first, the function Ψ should be positive, and second, at least one of the functions f_1 or f_2 should be negative. Figure 2 illustrates the situation.

The algorithm for finding the next collision time is straightforward. We move all the ellipses in time steps of length $\tau^{(0)}$ until an overlap between two ellipses is detected. Suppose this occurs in timestep s (note there is no overlap after time step $s-1$), therefore we bring back all the ellipses one timestep backward in time. From this time origin, i.e., $t = (s-1)\tau^{(0)}$, we move the system with a shorter time step $\tau^{(1)} = \frac{\tau^{(0)}}{\lambda}$ ($\lambda > 1$). We proceed with $\tau^{(1)}$ until we encounter an overlap. We repeat this procedure in a while loop until the time step becomes less than a given tolerance. Consequently, the ellipses become very close to each other and can be regarded in touch [48]. Then we update the velocity and angular velocity of the colliding ellipses and proceed to the next collision event. Before closing this section, we would like to mention that for ellipses the distance of closest approach has been analytically evaluated and may be used as an alternative scheme for finding the collision time [51].

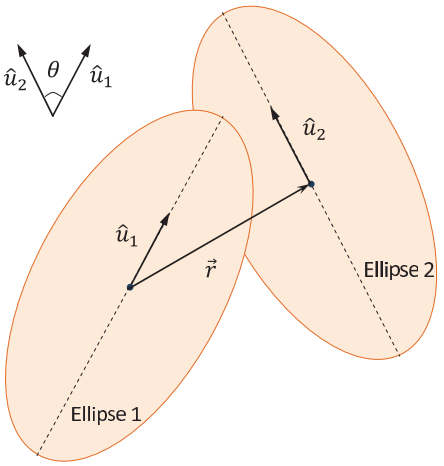

FIG. 2. (Color online) Overlap between two ellipses.

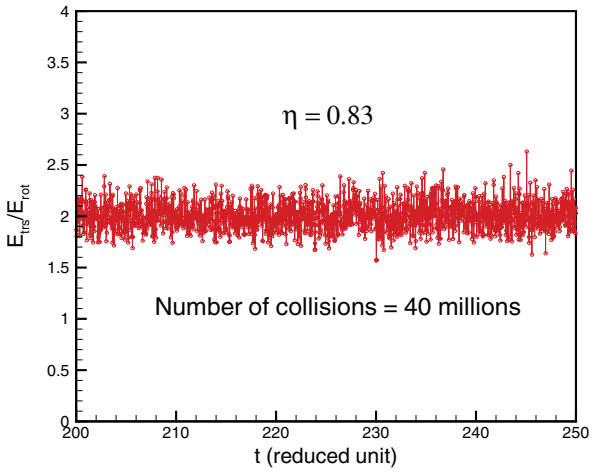

FIG. 3. (Color online) Time series (for a limited window of time) of the ratio between translational and rotational kinetic energies $\frac{E_{\rm trs}}{E_{\rm rot}}$ at packing fraction $\eta = 0.83$.

III. MOLECULAR DYNAMICS SIMULATION

A. Static properties

We have simulated the dynamics of a 2D hard ellipses fluid in NVE ensemble with the method explained in Sec. II. Periodic boundary condition is imposed. The sizes of our rectangular simulation box are $L_x = 30$ and $L_y = 45$. The packing fraction (total area covered by the ellipses) is defined as $\eta = \frac{N\pi ab}{L_x L_y}$, where N is the number of ellipses. Note πab is the area of an ellipse. The total energy of the system E (entirely kinetic) is divided into two segments of translational $E_{\rm trs}$ and rotational $E_{\rm rot}$. After a sufficient time, the system reaches to a thermal equilibrium in which the ratio $\frac{E_{\rm trs}}{E_{\rm rot}}$ becomes steady around two according to the classical equipartitioning of energy among degrees of freedom (two translational and one rotational). We remark that due to lack of any energy scale in the potential energy between ellipses, the temperature T appears as an overall multiplicative factor in thermodynamic quantities such as pressure and free energy. Thus, the state of the system trivially depends on temperature and hence energy. Nevertheless, E determines the time scale τ. In the thermal unit we have $\tau = a\sqrt{\frac{m}{k_B T}}$. We have taken the initial energy per particle $\frac{E}{N} = 1.5$ in our simulations, which corresponds to $k_B T = 1$. Figure 3 depicts the time evolution of $\frac{E_{\rm trs}}{E_{\rm rot}}$ for a densely packed case with $\eta = 0.83$.

The distribution of linear and angular velocities are exhibited in Fig. 4. According to the equipartition theorem, $P(v)$ is Maxwell-Boltzmannian, whereas $P(\omega)$ is Gaussian in the limit where the particle numbers become large. Despite the limited number of ellipses, the computed distributions considerably resemble the theoretical ones.

A useful quantity to explore is the average number of collisions per unit time Γ that an ellipse experiences. In Refs. [34] and [35] it is argued that Γ has a linear dependence on number density ρ in a 3D gas of hard needles ($\kappa \to \infty$). We have computed the dependence of Γ on η in Fig. 5. In fact, Γ shows a highly nonlinear behavior and drastically increases when η exceeds beyond 0.5. An exponential fit gives $\Gamma = 0.127e^{6.6\eta}$, whereas a power law fit yields $\Gamma = 47.4\eta^{3.47}$. In our previous work [43], in which a 2D gas of hard needles is investigated ($\kappa \to \infty$), it is found that Γ increases linearly when number density is increased.

The system equation of state, i.e., dependence of pressure P on the η is sketched in Fig. 6. More precisely, we have sketched

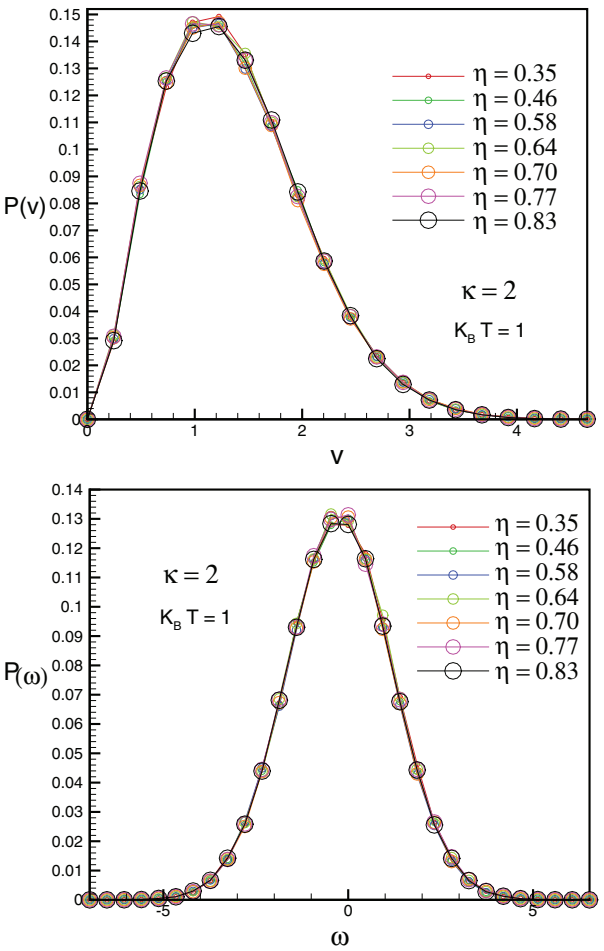

FIG. 4. (Color online) Distribution functions $P(v)$ and $P(\omega)$. For linear velocity the distributions is Maxwellian. $P(\omega)$ is Gaussian and centered at $\omega = 0$.

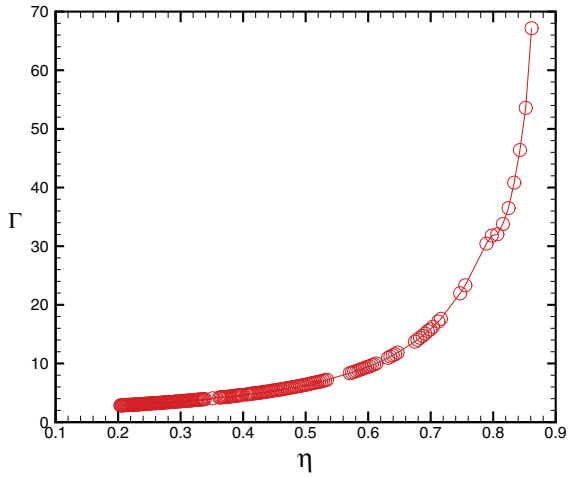

FIG. 5. (Color online) Collision frequency Γ vs. η for aspect ratio $\kappa = 2$. The dependence is nonlinear in contrary to the 3D gas of hard needles investigated in Refs. [34] and [35] and 2D hard needles gas investigated in Ref. [43]. Line is for eye help.

$P^* = \frac{\pi abP}{kT}$ versus η. In fact, P^* shows a rapid increase when η becomes large. Our results are in accordance with those obtained via Monte Carlo simulation [26,32] and density functional approach [29]. An exponential fit gives $P^* = 0.056e^{7.74\eta}$, whereas a power law fit yields $P^* = 58.63\eta^{4.08}$. We see substantial difference between 2D needles system and 2D ellipses systems. In Ref. [43], the pressure P for the 2D needles fluid shows a linear behavior with a slope in and intermediate number density.

B. Dynamics in positional and rotational degrees of freedom

It would be illustrative to look at some temporal autocorrelation functions both in position and rotation degrees of freedom. In Fig. 7 we exhibit the velocity autocorrelation function. Similar to two- and three-dimensional gas of hard needles [34,35,38,43], velocity auto correlation of 2D ellipse fluid decreases quickly in time. The denser the fluid, the slower

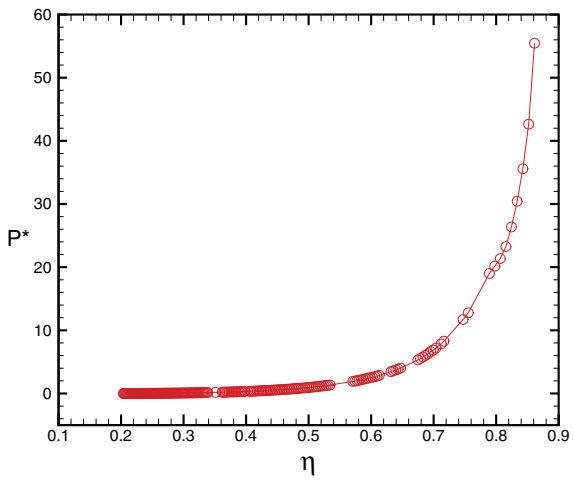

FIG. 6. (Color online) System pressure P^* vs. η. Line is for eye help.

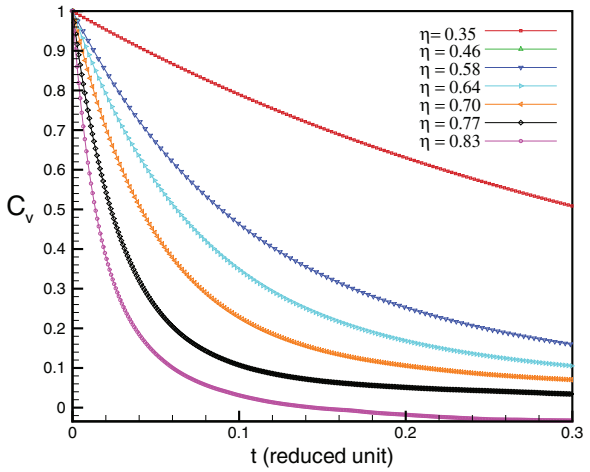

FIG. 7. (Color online) Temporal velocity auto correlation function for various values of η. Two time scales are identified for large packing fractions.

the decrease will be. This slowing down can be attributed to the onset of isotropic-nematic phase transition. The interesting point is that for the dense fluid, the temporal autocorrelation becomes negative.

Figure 8 exhibits the angular velocity autocorrelation function for various values of η. Analogous to linear velocity, the angular velocity temporal autocorrelation undergoes a sharper decrease when η increases. Similar to linear velocity, for large η and large enough time the temporal correlation becomes negative. To gain more insight into the nature of angular temporal organization of the system, we explore the autocorrelation between longitudinal and transverse decomposition of CM velocity. These quantities are defined as follows:

$$C_{||}(t) = \frac{1}{\langle v^2(0)\rangle}\langle \vec{v}(t)\cdot\hat{u}(0)\vec{v}(0)\cdot\hat{u}(0)\rangle, \tag{3}$$

$$C_{\perp}(t) = \frac{1}{\langle v^2(0)\rangle}\langle \vec{v}(t)P\vec{v}(0)\rangle. \tag{4}$$

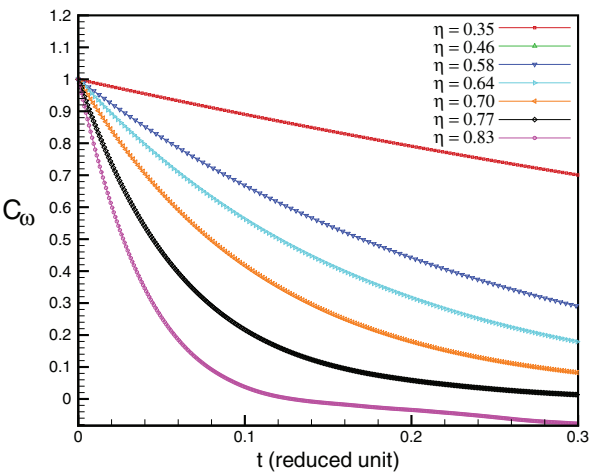

FIG. 8. (Color online) Temporal angular velocity auto correlation function for various values of η.

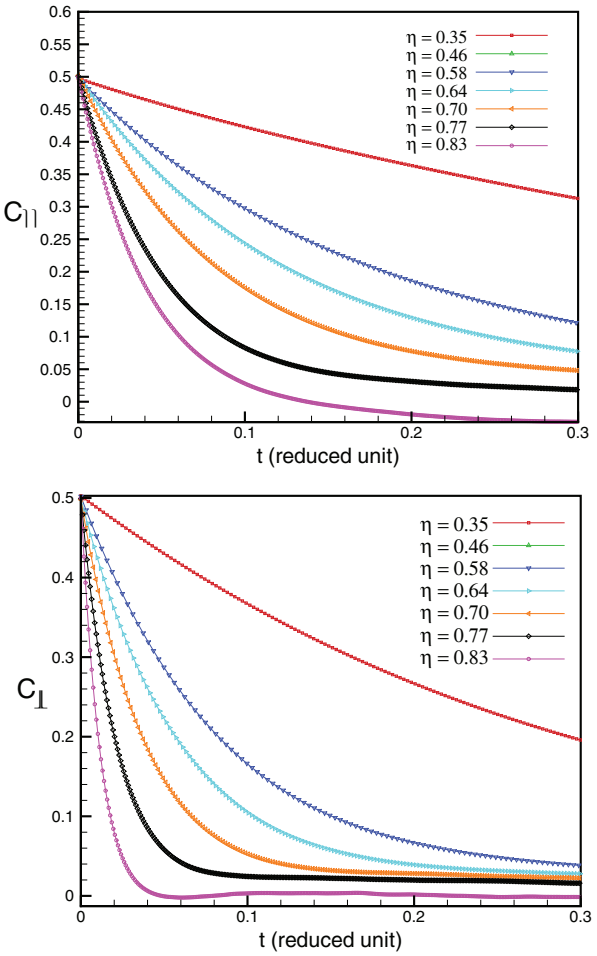

FIG. 9. (Color online) Temporal dependence of longitudinal and transverse components of velocity ACF. Longitudinal component exhibits a slower decay, which is due to direction of impulsive force between needles.

$\hat{u}$ denotes the unit vector along the ellipse major axis and the matrix $P = 1 - \hat{u}(0)\hat{u}^t(0)$ is the projection operator. We remark that $C_{||}(t)$ and $C_{\perp}(t)$ are such normalized that their sums gives C_v. In Fig. 9 we exhibit the temporal dependence of $C_{||}(t)$ and $C_{\perp}(t)$ for various densities. The observation of negative value for the correlation at long times, especially in $C_{||}(t)$, has been observed for the 3D ellipsoids or revolution [23].

Now let us consider the single particle temporal autocorrelation of the second-order angular-order parameter $C_2(t)$. This quantity is defined as follows [22]:

$$C_2(t) = \langle P_2(\hat{u}(t) \cdot \hat{u}(0)) \rangle, \tag{5}$$

in which P_2 is the second-order Legendre polynomial. Decay of this function implies that relaxation of orientational degrees of freedom has taken place. Figure 10 shows the temporal dependence of $C_2(t)$.

In low packing fractions we see a fast decay, which can be attributed to the fluid-like behavior. By increasing η we observe that the temporal behavior becomes slow and two characteristic time scales emerge. This confirms the nontrivial role played by the angular degree of freedom and can be associated to

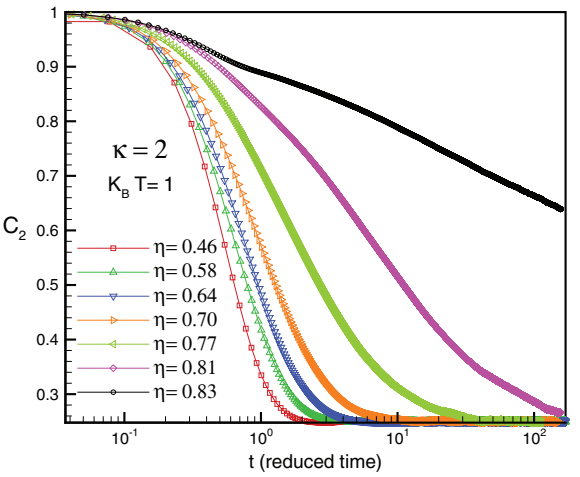

FIG. 10. (Color online) Temporal dependence of C_2 at various packing fractions η (semilog scale).

the onset of isotropic-nematic transition. Our results show clear evidence of slowing down of molecular rotation. We emphasize that simulation on larger system is needed to ensure the persistence of such large temporal correlations. The last temporal quantity we discuss in Fig. 11 is the intermediate self-scattering function $F_s(q,t)$.

Decay of $F_s(q,t)$ indicates that structural relaxation has occurred on the length scale set by q. Here also we observe that by increasing η the intermediate scattering function $F_s(q,t)$ persists longer in time. It seems that for a large enough packing fraction, a plateau region emerges on intermediate time scales, which could be indicative of glassy dynamics. The existence of plateau regions and the associated two-step decay in $F_s(q,t)$ has been verified by MC and MD simulations for 3D ellipsoidal system [8].

C. Static structural properties

We now wish to turn into the issue of structural characteristics of the system. We have obtained and explored various quantities, which are shown and discussed in order. First, we

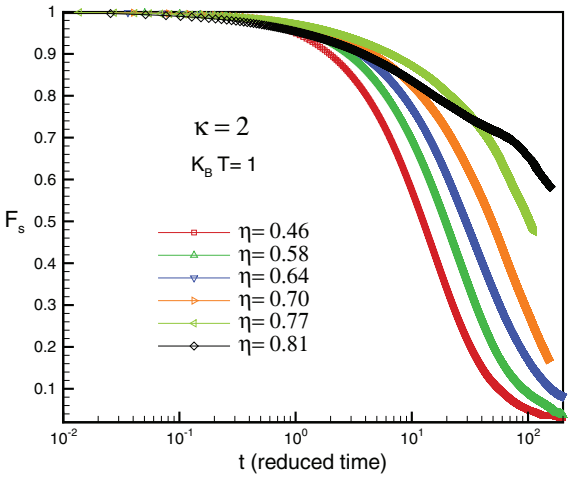

FIG. 11. (Color online) Time-dependence of the intermediate self-scattering function $F_s(q,t)$ at $q = 3$.

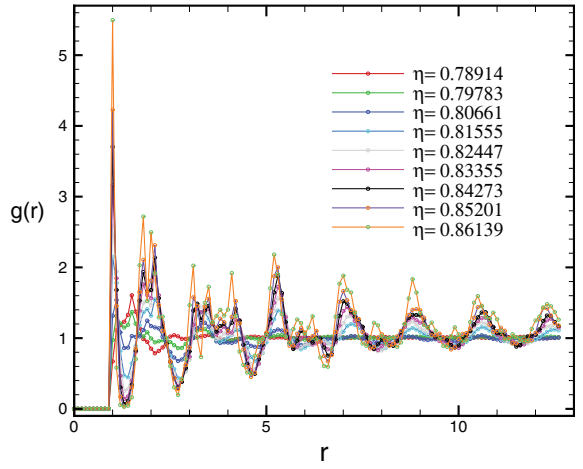

FIG. 12. (Color online) Dependence of $g(r)$ on r at a number of packing fractions.

consider radial distribution function $g(r)$ shown in Fig. 12 for various packing fractions. For completeness we define $g(r)$ as follows:

$$g(r) = (1/\eta N)\left\langle \sum_{i=1}^{N}\sum_{j\neq i}^{N} \delta(\vec{r} - \vec{r}_{ij}) \right\rangle. \tag{6}$$

$g(r)$ shows some oscillations in r and becomes almost constant at $r = 4$, irrespective of η. The oscillations amplitudes decrease in distance and can be attributed to the weak degree of spatial order in the system. The needle gas, on the contrary, does not show such oscillations and its $g(r)$ approaches to unity without showing any significant amplitude fluctuations. The absence of such fluctuations and prominent peaks demonstrates that from the positional point of view the 2D gas of hard needles has no ordering. This is expected because there is no excluded volume in hard needles, which forbids the formation of positional ordering. Contrary to hard needles, in the hard-disk fluid one observes similar $g(r)$, especially near the freezing point [52].

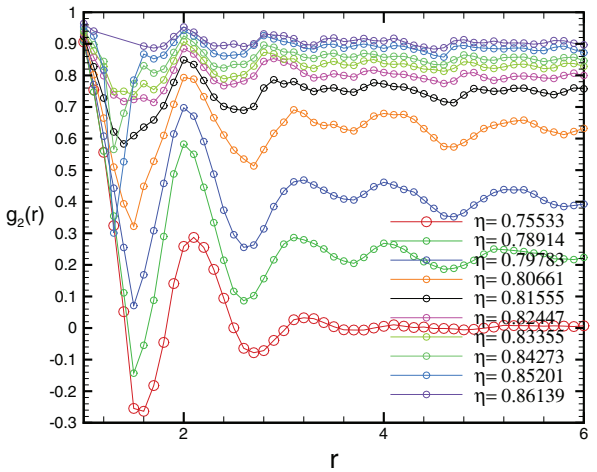

FIG. 13. (Color online) Dependence of $g_2(r)$ on r for various packing fractions.

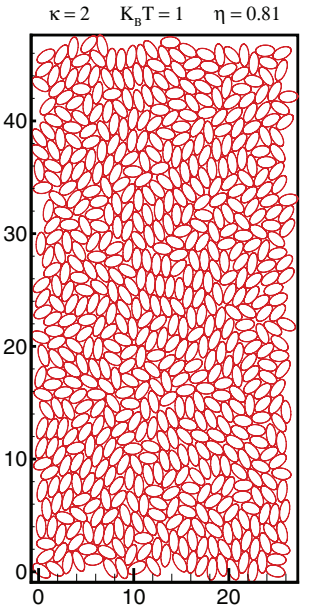

FIG. 14. (Color online) A snapshot at $\eta = 0.81$.

However, the ellipse fluid seems to possess some degrees of positional ordering. Simulations with larger number of ellipses is necessary to confirm this conjecture. We note that the existence of excluded volume effect distinguishes the positional features of the ellipse gas to ideal gas in which there is no excluded volume and correlations. Next we consider the angular spatial correlation function $g_2(r)$. This quantity is defined as follows [21]:

$$g_2(r) = \langle \cos(2[\theta(r) - \theta(0)]) \rangle. \tag{7}$$

The average is over all ellipses having CM-to-CM distance r from each other. Angles are measured with respect to a fixed axis, here Ox. Figure 13 plots the dependence of $g_2(r)$ versus r.

Similar to the radial distribution function $g(r)$, we see spatial oscillations with large amplitudes, which can be associated to orientational ordering in the system. The amplitude of oscillations become enhanced when η is increased. The dependence of $g_2(r)$ is totally different in nature with needle gas. In Ref. [43] we have shown, by MD simulations, that in the needle fluid $g_2(r)$ decreases from one toward zero without any noticeable fluctuations. For small number density of needles, the decrease is faster than algebraic but for higher densities $g_2(r)$ shows an algebraic decay. In our ellipses case, even for large packing fractions the angular correlation becomes negligible for $\eta > 0.6$. In contrast to needle gas, we infer that absence of algebraic decay of $g_2(r)$ diminishes the possibility of slow dynamics and angular structural arrest. The fluctuations of $g_2(r)$ resembles the radial bond orientational correlation function $g_6(r)$ in the hard disks problem [53]. Figures 14 and 15 exhibit two snapshots associated to $\eta = 0.81$ and $\eta = 0.85$, respectively.

IV. ORIENTATIONAL ORDERING

In order to explore the orientational ordering of the system, we first computed the angular order parameter S, introduced

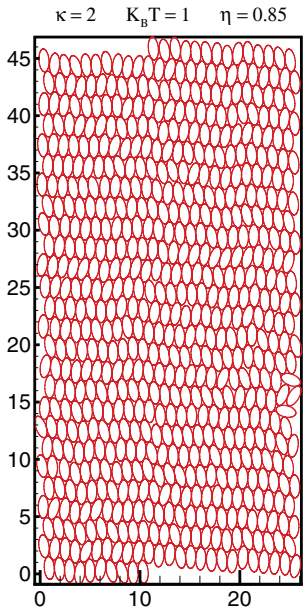

FIG. 15. (Color online) A snapshot at $\eta = 0.85$.

in Ref. [26], which is defined as follows:

$$S = \frac{1}{N^2} \sum_{i,j} \langle \cos 2(\theta_i - \theta_j) \rangle. \tag{8}$$

Note θ_i denotes the angle of ellipse i major axis with respect to x axis and $\langle\rangle$ means time averaging. Figure 16 exhibits the time evolution S for the packing fraction $\eta = 0.83$. To see higher packing of ellipses, see Ref. [54]. As you see after sufficient time the average of S becomes zero, which means there is no orientational ordering in the system.

The definition of the angular order parameter given in Eq. (8) is quite specific. Another definition which is frequently used in the literature is given below:

$$q = \frac{1}{N} \left\langle \sum_{i=1}^{N} \cos(2\theta_{i,n}) \right\rangle. \tag{9}$$

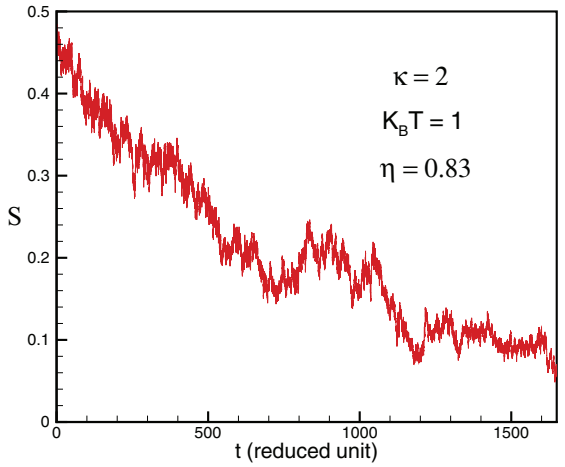

FIG. 16. (Color online) Temporal evolution of angular order parameter S at $\eta = 0.83$.

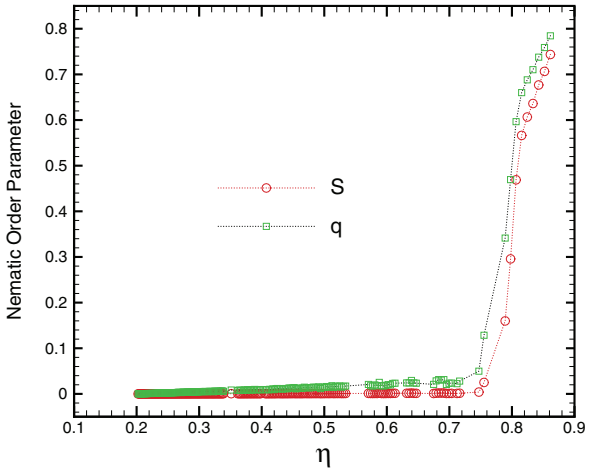

FIG. 17. (Color online) Nematic order parameter q and Baron order parameter S vs. packing fraction η.

Here, $\theta_{i,n}$ is the angle between ith ellipse and the nematic direction. To compute the nematic direction a tensor order parameter Q is defined:

$$Q_{\alpha,\beta} = \frac{1}{N} \left\langle \sum_{i=1}^{N} [2u_\alpha(i)u_\beta(i) - \delta_{\alpha,\beta}] \right\rangle. \tag{10}$$

α and β take x, y and $u_\alpha(i)$ represents the α Cartesian component of the unit vector specifying the direction of ith ellipse with x axis. The eigenvector corresponding to the largest eigenvalue of matrix Q gives the nematic direction. We remark that in the thermodynamic limit the eigenvalues of tensor Q become $\pm q$. In Fig. 17 the dependence of S and q on η is shown. Our findings are in accordance with those obtained via MC simulations done by Cuesta and Frenkel [32]. We observe that there is no orientational ordering in the vicinity of solid phase, which indicates the absence of a nematic phase. The absence of nematic phase for $k = 2$ hard ellipses has been confirmed via the MC simulation of Cuesta and Frenkel in Ref. [32]. In contrast to $k = 2$, the more elongated ellipses having $k = 4$ and $k = 6$ were shown to posses nematic phase. Moreover, the MC simulations show that nematic-solid transition is first order for $k = 6$ but continuous for $k = 4$ [32].

V. TRANSPORT PROPERTIES

In this section we report our results for the transport properties and orientational structure of the system. We begin with translational diffusion coefficient $D_{\rm trs}$ defined as follows:

$$D_{\rm trs} = \lim_{t\to\infty} \frac{1}{2dNt} \sum_{i=1}^{N} \langle |\vec{r}_i(t) - \vec{r}_i(0)|^2 \rangle. \tag{11}$$

The term in the bracket is the translational mean-square displacement (MSD) $\langle (\Delta\vec{r})^2 \rangle$. Here the spatial dimension d is two and the average is doubly taken over trajectories of ellipses CM and time origins. Figure 18 sketches the time dependence of the translational MSD.

For small $\eta < 0.7$ and after a ballistic regime, one recovers normal diffusive behavior. This confirms that from a translational viewpoint, the system resembles a structureless gas. when η goes beyond 0.7, we observe the MSD exhibits

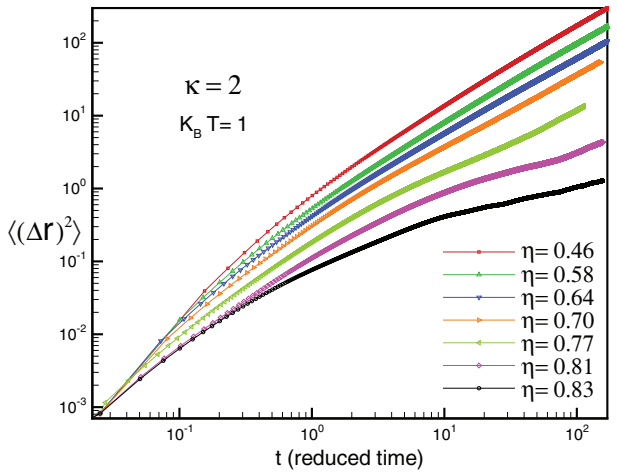

FIG. 18. (Color online) Time dependence of $\langle(\Delta\vec{r})^2\rangle$ at various packing fractions. For the fluid case where η is small we see a two-state behavior from ballistic to normal diffusion. When η is increased we see three temporal regimes.

three-stage behavior in time and for large times the MSD is deviated from the normal diffusion. This can be associated to slow dynamics. Obviously, longer simulation with larger number of ellipses is needed to confirm this picture. Figure 19 plots a CM trajectory of a typical ellipse at three packing fractions $\eta = 0.46$, 0.77, and 0.83.

Three distinctive kinds of motion can be identified: diffusion (isotropic fluid phase), entanglement among neighboring ellipses (solid phase), and channeling (intermediate phase). At low η the motion resembles a normal diffusion. At higher η a channeling type of motion emerges during which an ellipse moves along a path along its axis direction without much deviation. From time to time the ellipse is entangled by its adjacent ellipses. For higher η, the topological constraints in two dimensions leads to the third type of motion, i.e., entanglement. In this phase, the system becomes solid and each ellipse only fluctuates, with a small amplitude, around its equilibrium position. Let us now explore the rotational diffusion and particularly its coefficient $D_{\rm rot}$. In contrast to positional, rotational diffusion seems to be of a different nature. We have computed the rotational diffusion coefficient by the following definition:

$$D_{\rm rot} = \lim_{t\to\infty} \frac{1}{2\zeta N t} \sum_{i=1}^{N} \langle|\theta_i(t) - \theta_i(0)|^2\rangle. \qquad (12)$$

Analogously, the bracketed term denotes the angular mean-square displacement $\langle(\Delta\theta)^2\rangle$ and ζ is the number of angular degrees of freedom (here, $\zeta = 1$). Figure 20 exhibits the time dependence of $\langle(\Delta\theta)^2\rangle$.

We see a significant difference compared to the translational diffusion. At high η, the rotational MSD exhibits a three-stage regime in time, which can be attributed to an angular cage effect similar to the cage effect in the translational dynamics of simple liquids. The caging effect emerges when the density becomes larger than a density around $\eta_c = 0.83$. Our findings are supportive of the existence of slow dynamics in two dimensions, even when the translational degree of freedom is

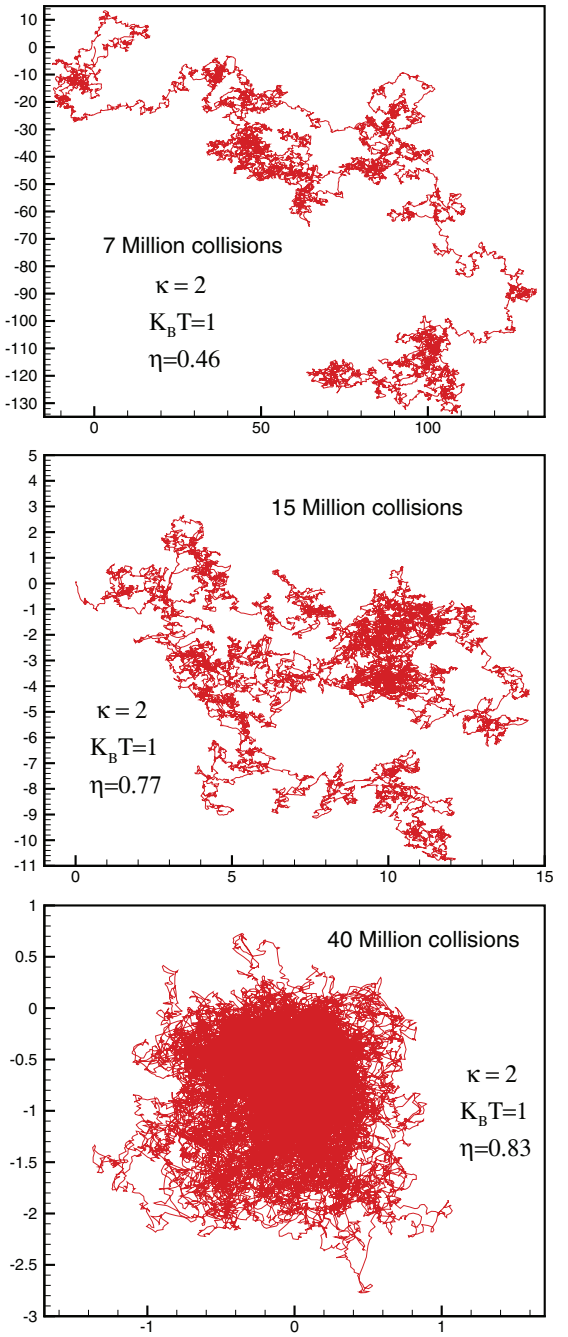

FIG. 19. (Color online) CM trajectory of a typical ellipse at $\eta = 0.46$,0.77 and 0.83. Look at the scales.

released. The orientational behavior of the ellipse gas is similar to needle gas [43], where slow dynamics was observed in the angular motion. However, the existence of a plateau region is more apparent in the ellipse case in comparison to needle system. From the positional point of view, the ellipse gas seems to have more significant spatial organization. It should be emphasized that further extensive simulation with a larger system size is crucially needed to confirm these conclusions. Unfortunately, the amount of computer time increases dramatically with system size. Finally, we discuss the dependence of translational and rotational diffusion constants on η. Let us first discuss the translational motion. In Fig. 21 we show the

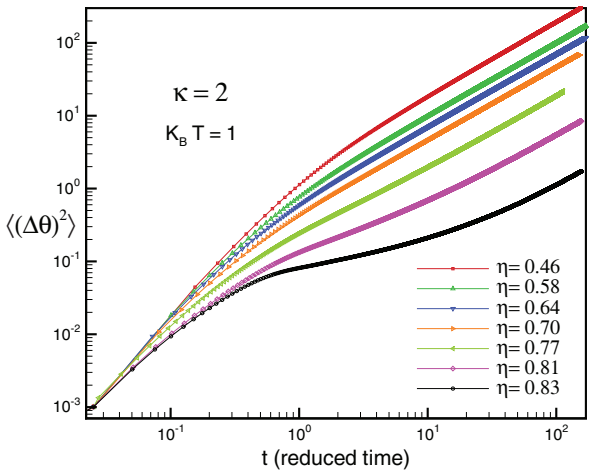

FIG. 20. (Color online) Time dependence of $\langle(\Delta\theta)^2\rangle$ for various values of η. For small packing fractions we see a ballistic regime followed by a diffusive one. When η is increased beyond 0.8 we see three temporal regimes. The intermediate one corresponds to slow dynamics in orientational behavior.

dependence of $D_{\rm trs}$ on η. As you can see, $D_{\rm trs}$ is a decreasing function of η. In the needle system, $D_{\rm trs}$ shows a sharper decrease with number density and nicely fits to an exponential function [43].

Eventually, Fig. 22 exhibits the dependence of the rotational diffusion constant $D_{\rm rot}$ on η. $D_{\rm rot}$ is also a decreasing function of η. The rate of decrease is sharper than the positional diffusion constant $D_{\rm trs}$. A power law fit gives $D_{\rm rot} = 0.005\eta^{-5.01}$. It should be noted our data for large packing fractions are less reliable than the small packing ones. We are not aware of any analytical results for the translational and rotational diffusion constants to compare our findings with them. For the needle gas, however, there are analytical results. In 3D and based on scaling arguments it can be concluded that within the Doi-Edward theory $D_{\rm rot}$ scales as ρ^{-2}. MD simulations for a 3D gas of hard needles gives the dependence of $D_{\rm rot}$ on density as $D_{\rm rot} \sim \rho^{-\beta}$ with $\beta \in$

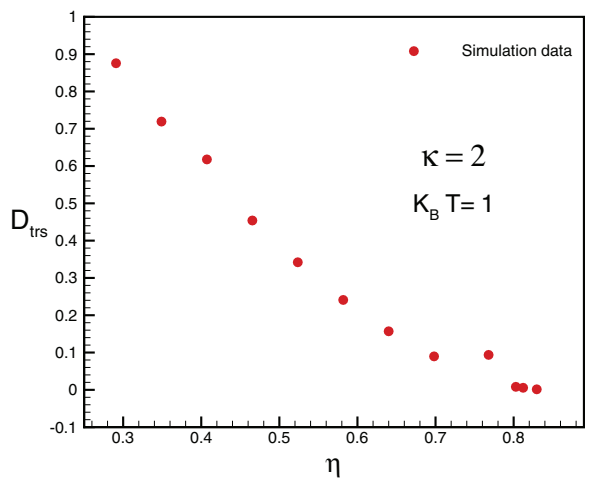

FIG. 21. (Color online) Dependence of $D_{\rm trs}$ on the packing fraction η.

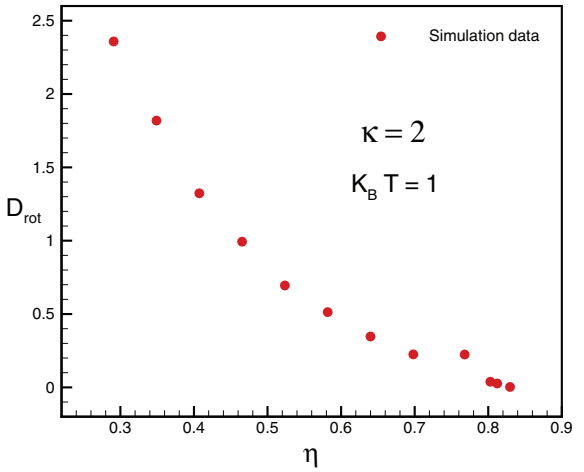

FIG. 22. (Color online) Dependence of $D_{\rm rot}$ on the packing fraction η.

[1.8,2.2] [34]. For a 2D needle system, MD simulations gives $D_{\rm rot} \sim \rho^{-3.6}$ [43].

VI. SUMMARY AND CONCLUDING REMARKS

To summarize, we have simulated the dynamics of a two-dimensional system of hard ellipses with aspect ratio $\kappa = 2$ by event-oriented molecular dynamics in NVE ensemble. The dynamic properties of the system seem nontrivial. Analogous to our previous findings in a 2D needle system, many of the temporal autocorrelation functions, both translational and rotational, exhibit a sort of slow dynamics and multistep relaxation. The most interesting feature of the system, which has not been explored earlier, is the existence of three regimes in the temporal behavior of the angular mean-square displacement. This can be attributed to slow dynamics and possibly the angular glassy dynamics in the system. From the spatial viewpoint, the ellipse system is much more organized than the needle system, which seems almost structureless. Our findings show that relaxation of the translational degrees of freedom does not smear out angular slow dynamics. The dependence of translational and rotational diffusion coefficients on the packing fraction have been computed and compared to existing results obtained by Monte Carlo simulations.

ACKNOWLEDGMENTS

This work has been funded by Iran National Science Foundation under Grant No. 844169. We appreciate enlightening discussions with Daan Frenkel from Cambridge University. Fruitful discussions are acknowledged with Peter Palffy-Muhoray and Xiaoyu Zheng from Kent University, Reza Khordad from Shiraz University, Tanja Schilling from Luxemburg University, Amir Hossein Fathollahi from Alzahra University in Tehran, and Hossein Fazli from the Institute of Advanced Studies in Basic Sciences (IASBS) in Zanjan. Special thanks are given to Asgar Ghorbani for useful suggestions and an anonymous referee for his fruitful and enlightening comments. We have benefited much from the computational facilities at IASBS in Zanjan. We express our gratitude to this institute

and especially to its computer coordinator Ehsaan Nedaaee. M.E.F. is thankful to Amir-o Do'leh for his encouragement.

APPENDIX A: DYNAMICS OF COLLISION

In this Appendix we intend to obtain the post-collision velocities (linear and angular) of two colliding ellipses in terms of pre-collision ones provided the coordinates of the collision point are known. We denote the coordinates of the collision point between two identical ellipses by $\mathbf{r}^* = (x^*, y^*)$. We arbitrarily refer to one of the ellipses as *collider* and the to the other one as *partner*. Centers of collider and partner ellipses are shown by $\mathbf{R}_c = (X_c, Y_c)$ and $\mathbf{R}_p = (X_p, Y_p)$, respectively. The pre-collision center of mass velocity and the angular velocity (around z axis) of the collider ellipse is exhibited by $\mathbf{v}_c$ and ω_c. Analogously, $\mathbf{v}_p$ and ω_p show the corresponding velocities of the partner ellipse. The post-collision velocities are primed. Moreover, let $\mathbf{r}_c$ and $\mathbf{r}_p$ denote the vectors connecting the collision point to the centers of collider and partner ellipses, respectively (see Fig. 1 for illustration). Conservation of linear momentum implies

$$\mathbf{v}_c + \mathbf{v}_p = \mathbf{v}'_c + \mathbf{v}'_p. \tag{A1}$$

Conservation of energy gives

$$mv_c^2 + I\omega_c^2 + mv_p^2 + I\omega_p^2 = mv_c'^2 + I\omega_c'^2 + mv_p'^2 + I\omega_p'^2. \tag{A2}$$

Next we write the conservation of angular momentum with respect to the z axis passing at the collision point:

$$\begin{aligned} &m(\mathbf{r}_c \times \mathbf{v}_c + \mathbf{r}_p \times \mathbf{v}_p) + I(\omega_c + \omega_p)\hat{k} \\ &\quad = m(\mathbf{r}_c \times \mathbf{v}'_c + \mathbf{r}_p \times \mathbf{v}'_p) + I(\omega'_c + \omega'_p)\hat{k}. \end{aligned} \tag{A3}$$

Note we have six unknowns v'_{cx}, v'_{cy}, v'_{px}, v'_{py}, ω'_c, and ω'_p, but so far we have only four equations [two from Eq. (A1) and one for each of Eqs. (A2) and (A3)]. We need two further independent equations. One of them can be obtained from the direction of the exerted impulsive forces between ellipses. As a matter of fact, if there is no friction the exerted force will be along the unit normal vector on the ellipse surface at the collision point. We now define another reference frame, with a positive x axis (denoted by x') along the unit normal vector $\hat{n}$ on the collider ellipse (see Fig. 1). Choosing $\hat{k}' = \hat{k}$ and assuming the primed reference system is right-handed, we simply find $\hat{y}' = \hat{k} \times \hat{x}'$. From now on we refer to this reference frame as *collision frame*. As you will shortly see, it would be easier to find post-collision quantities in the collision frame. The components of vectors along the impulsive force will be denoted by $||$ subscript, whereas the components perpendicular to it will be denoted by $\perp$ subscript. Since the impulsive forces are along $\hat{n}$, the perpendicular components of post-collision linear velocities remain unchanged and only the parallel components will be affected by the collision. Therefore, we have

$$v'_{c\perp} = v_{c\perp}; \quad v'_{p\perp} = v_{p\perp}. \tag{A4}$$

Equation (A4) gives one of the remaining equations. Having Eq. (A4) in mind, Eq. (A1) becomes

$$v'_{c\parallel} + v'_{p\parallel} = v_{c\parallel} + v_{p\parallel}. \tag{A5}$$

Now we have four unknowns $v'_{c\parallel}$, $v'_{p\parallel}$, ω'_c, and ω'_p but three equations, i.e., Eqs. (A2), (A3), and (A5). To find the last equation we utilize the concepts of linear and angular impulses. Let $\mathbf{I}_{p\to c}$ be the linear impulse exerted on the collider ellipse by the partner ellipse. Similarly, $\mathbf{I}_{c\to p}$ is the linear impulse exerted on the partner ellipse by the collider ellipse. We have

$$\mathbf{I}_{p\to c} = \int \mathbf{F}_{p\to c}dt = \Delta\mathbf{p}_c; \quad \mathbf{I}_{c\to p} = \int \mathbf{F}_{c\to p}dt = \Delta\mathbf{p}_p, \tag{A6}$$

where $\Delta\mathbf{p}_c$ and $\Delta\mathbf{p}_p$ are the changes of linear momentum of collider and partner ellipses during the collision. In a similar manner, we can define angular impulses as follows:

$$\mathbf{J}_{p\to c} = \int \vec{\tau}_{p\to c}dt = \Delta\mathbf{L}_c; \quad \mathbf{J}_{c\to p} = \int \vec{\tau}_{c\to p}dt = \Delta\mathbf{L}_p, \tag{A7}$$

where $\vec{\tau}_{p\to c}$ and $\vec{\tau}_{c\to p}$ are the torque exerted on the collider and partner ellipses during the collision, respectively. Furthermore, $\Delta\mathbf{L}_c$ and $\Delta\mathbf{L}_p$ are the angular momentum change of the collider and the partner ellipses. To proceed further, we take the cross product of $\hat{j}'$ with the first part of Eq. (A7) and find

$$\mathbf{I}_{p\to c} = \frac{I(\omega'_c - \omega_c)}{r_{c\perp}}\hat{i}'. \tag{A8}$$

Taking the cross product of the second part with $\hat{j}'$ gives the following equation:

$$\mathbf{I}_{c\to p} = \frac{I(\omega'_p - \omega_p)}{r_{p\perp}}\hat{i}'. \tag{A9}$$

Comparing Eqs. (A8) and (A9) we find

$$\frac{\omega'_c - \omega_c}{\omega'_p - \omega_p} = -\frac{r_{c\perp}}{r_{p\perp}}. \tag{A10}$$

Equation (A10) is the fourth equation we were seeking. Let us now solve these four equations. We write $\mathbf{r}_c$ and $\mathbf{r}_p$ in the collision frame as follows:

$$\mathbf{r}_c = r_{c\parallel}\hat{i}' + r_{c\perp}\hat{j}'; \quad \mathbf{r}_p = r_{p\parallel}\hat{i}' + r_{p\perp}\hat{j}'. \tag{A11}$$

Similarly, we have

$$\mathbf{v}_c = v_{c\parallel}\hat{i}' + v_{c\perp}\hat{j}'; \quad \mathbf{v}_p = v_{p\parallel}\hat{i}' + v_{p\perp}\hat{j}'. \tag{A12}$$

Replacing Eqs. (A11) and (A12) into Eq. (A3), we find

$$\begin{aligned} &I(\omega_c + \omega_p) - m(r_{c\perp}v_{c\parallel} + r_{p\perp}v_{p\parallel}) \\ &\quad = I(\omega'_c + \omega'_p) - m(r_{c\perp}v'_{c\parallel} + r_{p\perp}v'_{p\parallel}). \end{aligned} \tag{A13}$$

In order to simplify the rest of the calculations, we introduce

$$\Delta v_{c\parallel} = v'_{c\parallel} - v_{c\parallel}; \quad \Delta v_{p\parallel} = v'_{p\parallel} - v_{p\parallel}; \quad A = \frac{r_{c\perp}}{r_{p\perp}} - 1. \tag{A14}$$

With these notations, Eq. (A13) becomes

$$\omega'_c - \omega_c = \omega_p - \omega'_p + \frac{m}{I}r_{cp\perp}\Delta v_{c\parallel}. \tag{A15}$$

Solving Eqs. (A10) and (A15) yields

$$\omega'_p = \omega_p - \frac{m}{IA}r_{cp\perp}\Delta v_{c\parallel}, \tag{A16}$$

$$\omega'_c = \omega_c + \frac{m(A+1)}{IA}r_{cp\perp}\Delta v_{c\parallel}. \tag{A17}$$

We can also write

$$v'_{c\parallel} = v_{c\parallel} + \Delta v_{c\parallel}; \quad v'_{p\parallel} = v_{p\parallel} - \Delta v_{c\parallel}. \tag{A18}$$

Thus we see from Eqs. (A16)–(A18) that if one can obtain $\Delta v_{c\parallel}$ in terms of pre-collision quantities, all the unknowns are obtained. For this purpose we use Eq. (A2), which has not been utilized so far. Replacing all primed quantities, except $v'_{c\parallel}$, in terms of pre-collision quantities, we arrive at a quadratic equation (not written here) for $v'_{c\parallel}$. The answers turn out to be

$$v'_{c\parallel} = v_{c\parallel}; \quad v'_{c\parallel} = v_{c\parallel} - \frac{v_{c\parallel} - v_{p\parallel} + \frac{r_{cp\perp}}{A}(\omega_c + A\omega_c - \omega_p)}{1 + \frac{m}{2IA^2}(A^2 + 2A + 2)r^2_{cp\perp}}. \tag{A19}$$

Obviously, the solution $v'_{c\parallel} = v_{c\parallel}$ is not acceptable because it implies no change in the ellipses status. The acceptable answer gives

$$\Delta v_{c\parallel} = \frac{v_{p\parallel} - v_{c\parallel} + \frac{r_{cp\perp}}{A}(\omega_p - A\omega_c - \omega_c)}{1 + \frac{m}{2IA^2}(A^2 + 2A + 2)r^2_{cp\perp}}. \tag{A20}$$

By substituting $\Delta v_{c\parallel}$ from Eq. (A20) into Eqs. (A16)–(A18), all the post-collision velocities will be given in terms of pre-collision ones. However, it should be noted that in Eq. (A20) the pre-collision quantities are expressed in the collision reference frame, which is instantaneous. For practical purposes, we should be able to express the pre-collision quantities in Eq. (A20) in the fixed reference frame. To this end, first we notice that ω_c and ω_p have the identical values in the collision and fixed frames because the problem is two-dimensional. For the other vectors, let us show the directions $\hat{i}'$ and $\hat{j}'$ by $\hat{n}$ and $\hat{\tau}$, respectively. In fact, $\hat{n}$ is the unit normal vector and $\hat{\tau}$ is the unit tangent vector at the collision point of collider ellipse (see Fig. 1). An arbitrary vector $\mathbf{Q}$ can be written in the fixed frame as follows:

$$\mathbf{Q} = Q_x\hat{i} + Q_y\hat{j}. \tag{A21}$$

This vector takes the following form in the collision frame:

$$\mathbf{Q} = (\mathbf{Q}\cdot\hat{n})\hat{n} + (\mathbf{Q}\cdot\hat{\tau})\hat{\tau} = Q_\parallel\hat{n} + Q_\perp\hat{\tau}. \tag{A22}$$

If the equation of partner and collider ellipses are $f_p(x,y) = 0$ and $f_c(x,y) = 0$, then $\hat{n}$ turns out to be

$$\hat{n} = \frac{\nabla f_c(x^*,y^*)}{|\nabla f_c(x^*,y^*)|}. \tag{A23}$$

The unit tangent vector $\hat{\tau}$ can be written as

$$\hat{\tau} = \hat{k}\times\hat{n} = \hat{k}\times(n_x\hat{i} + n_y\hat{j}) = -n_y\hat{i} + n_x\hat{j}. \tag{A24}$$

We are now able to express the components of $\mathbf{Q}$ in the collision frame in terms of n_x,n_y and its components in the fixed frame:

$$Q_\parallel = \mathbf{Q}\cdot\hat{n} = (Q_x\hat{i} + Q_y\hat{j})\cdot(n_x\hat{i} + n_y\hat{j}) = Q_xn_x + Q_yn_y, \tag{A25}$$

$$Q_\perp = \mathbf{Q}\cdot\hat{\tau} = (Q_x\hat{i} + Q_y\hat{j})\cdot(-n_y\hat{i} + n_x\hat{j}) = Q_yn_x - Q_xn_y. \tag{A26}$$

To find explicitly n_x and n_y, we note the equations of ellipses are (see Appendix B)

$$f_c(x,y) = A_c(x - X_c)^2 + B_c(y - Y_c)^2 + C_c(x - X_c)(y - Y_c) + D_c = 0, \tag{A27}$$

$$f_p(x,y) = A_p(x - X_p)^2 + B_p(y - Y_p)^2 + C_p(x - X_p)(y - Y_p) + D_p = 0. \tag{A28}$$

The coefficients turn out to be

$$A_c = e^2\cos^2\theta_c - 1; \quad B_c = e^2\sin^2\theta_c - 1; \quad C_c = e^2\sin 2\theta_c; \quad D_c = b^2, \tag{A29}$$

where θ_c is the angle between the major axis of collider with respect to x axis of fixed reference frame and $e = \sqrt{1 - \frac{b^2}{a^2}}$ is the ellipse eccentricity. By changing $c \to p$ we obtain coefficients for the partner ellipse. Furthermore, we obtain

$$\frac{\partial f_c}{\partial x}(x^*,y^*) = 2A_c(x^* - X_c) + C_c(y^* - Y_c), \tag{A30}$$

$$\frac{\partial f_c}{\partial y}(x^*,y^*) = 2B_c(y^* - Y_c) + C_c(x^* - X_c). \tag{A31}$$

By substituting Eqs. (A30) and (A31) into Eq. (A23), we find

$$n_x = \frac{2A_c(x^* - X_c) + C_c(y^* - Y_c)}{\sqrt{(x^* - X_c)^2\left(4A_c^2 + C_c^2\right) + (y^* - Y_c)^2\left(4B_c^2 + C_c^2\right) + 4C_c(x^* - X_c)(y^* - Y_c)(A_c + B_c)}}, \tag{A32}$$

$$n_y = \frac{2B_c(y^* - Y_c) + C_c(x^* - X_c)}{\sqrt{(x^* - X_c)^2\left(4A_c^2 + C_c^2\right) + (y^* - Y_c)^2\left(4B_c^2 + C_c^2\right) + 4C_c(x^* - X_c)(y^* - Y_c)(A_c + B_c)}}. \tag{A33}$$

Substitution of Eqs. (A32) and (A33) into Eqs. (A25) and (A26) gives the components of every vector in the collision frame in terms of its components in the fixed frame. Here are some examples:

$$r_{c\parallel} = \frac{r_{cx}[2A_c(x^* - X_c) + C_c(y^* - Y_c)] + r_{cy}[2B_c(y^* - Y_c) + C_c(x^* - X_c)]}{\sqrt{(x^* - X_c)^2\left(4A_c^2 + C_c^2\right) + (y^* - Y_c)^2\left(4B_c^2 + C_c^2\right) + 4C_c(x^* - X_c)(y^* - Y_c)(A_c + B_c)}}, \tag{A34}$$

$$r_{c\perp} = \frac{-r_{cx}[2B_c(y^* - Y_c) + C_c(x^* - X_c)] + r_{cy}[2A_c(x^* - X_c) + C_c(y^* - Y_c)]}{\sqrt{(x^* - X_c)^2\left(4A_c^2 + C_c^2\right) + (y^* - Y_c)^2\left(4B_c^2 + C_c^2\right) + 4C_c(x^* - X_c)(y^* - Y_c)(A_c + B_c)}}, \tag{A35}$$

$$v_{c\parallel} = \frac{v_{cx}[2A_c(x^* - X_c) + C_c(y^* - Y_c)] + v_{cy}[2B_c(y^* - Y_c) + C_c(x^* - X_c)]}{\sqrt{(x^* - X_c)^2\left(4A_c^2 + C_c^2\right) + (y^* - Y_c)^2\left(4B_c^2 + C_c^2\right) + 4C_c(x^* - X_c)(y^* - Y_c)(A_c + B_c)}}, \tag{A36}$$

$$v_{c\perp} = \frac{-v_{px}[2B_c(y^* - Y_c) + C_c(x^* - X_c)] + v_{py}[2A_c(x^* - X_c) + C_c(y^* - Y_c)]}{\sqrt{(x^* - X_c)^2\left(4A_c^2 + C_c^2\right) + (y^* - Y_c)^2\left(4B_c^2 + C_c^2\right) + 4C_c(x^* - X_c)(y^* - Y_c)(A_c + B_c)}}. \tag{A37}$$

APPENDIX B: COORDINATES OF THE COLLISION POINT

In this Appendix we show how to find the coordinates of the collision point if the collision time between two ellipses is known. Suppose two ellipses (labeled with numbers one and two) are apart from each other at $t = 0$. Center of mass of ellipse i is at $[x_i(0), y_i(0)]$ and its major axis makes angle $\theta_i(0)$ with respect to x axis ($i = 1,2$). Denoting the collision time by t^* the ellipse i configuration at the collision instant become $[x_i(t^*), y_i(t^*)]$ and $\theta_i(t^*)$ in which $x_i(t^*) = x_i(0) + v_{xi}t^*, y_i(t^*) = y_i(0) + v_{yi}t^*$ and $\theta_i(t^*) = \theta_i(0) + \omega_i t^*$. We denote $x_i(t^*), y_i(t^*)$ and $\theta_i(t^*)$ by x_i, y_i and θ_i for abbreviation. Moreover, the coordinates of the two foci of ellipse i turn out to be $(x_i \pm c\cos\theta_i, y_i \pm c\sin\theta_i)$, where $c = ea$. The equation of ellipse i then becomes

$$\sqrt{[x - (x_i + c\cos\theta_i)]^2 + [y - (y_i + c\sin\theta_i)]^2} + \sqrt{[x - (x_i - c\cos\theta_i)]^2 + [y - (y_i - c\sin\theta_i)]^2} = 2a. \tag{B1}$$

Squaring both sides, after lengthy but straightforward algebra we arrive at the following equation:

$$A_i(x - x_i)^2 + B_i(y - y_i)^2 + C_i(x - x_i)(y - y_i) + D_i = 0 \quad i = 1,2, \tag{B2}$$

where

$$A_i = e^2\cos^2\theta_i - 1; \quad B_i = e^2\sin^2\theta_i - 1; \quad C_i = e^2\sin 2\theta_i; \quad D_i = b^2. \tag{B3}$$

Since the collision point should satisfy the equations of both ellipses, we have

$$A_1(x^* - x_1)^2 + B_1(y^* - y_1)^2 + C_1(x^* - x_1)(y^* - y_1) + D_1 = 0, \tag{B4}$$

$$A_2(x^* - x_2)^2 + B_2(y^* - y_2)^2 + C_2(x^* - x_2)(y^* - y_2) + D_2 = 0. \tag{B5}$$

By solving Eqs. (B4) and (B5) we find the coordinates of the collision point x^* and y^*. By replacing x^* in terms of y^* and after very lengthy algebra we reach to the following quartic equation for y^*:

$$H(y^*)^4 + I(y^*)^3 + J(y^*)^2 + Ky^* + L = 0, \tag{B6}$$

where

$$H = C'^2; \quad I = D' - 4y_1C'^2; \quad J = 6y_1^2C'^2 - 3y_1D' + E'; \quad K = -4y_1^3C'^2 + 3y_1^2D' - 2y_1E' + F', \tag{B7}$$

$$L = y_1^4C'^2 - D'y_1^3 + E'y_1^2 - F'y_1 + G', \tag{B8}$$

in which

$$A' = 4A_1^2A_2^2(x_1 - x_2)^2 - 4A_1A_2^2D_1 + 4A_1^2D_2, \tag{B9}$$

$$B' = 4A_1C_2(A_1 - A_2)(x_1 - x_2), \tag{B10}$$

$$C' = A_2C_1^2 - 4A_1A_2B_1 + A_2C_2^2 + 4A_1^2B_2 - 2A_1C_2^2, \tag{B11}$$

$$D' = 2B'C' + 2C_2\left(4A_1B_1 - C_1^2\right)(A_1 - A_2), \tag{B12}$$

$$E' = B'^2 + 2A'C' + 4A_1A_2(x_1 - x_2)\left(4A_1B_1 - C_1^2\right), \tag{B13}$$

$$F' = 2A'B' + 8A_1D_1C_2(A_1 - A_2), \tag{B14}$$

$$G' = A'^2 + 16A_1^2A_2D_1(x_1 - x_2). \tag{B15}$$

We can solve Eq. (B6) by the Ferrari method (see mathematical handbooks such as Ref. [55]) and find y^*. Then x^* is found from the following quadratic equation:

$$x^* = \frac{-c_1(y^* - y_1) \pm \sqrt{c_1^2(y^* - y_1)^2 - 4A_1[D_1 + B_1(y^* - y_1)^2]}}{2A_1} + x_1. \tag{B16}$$

Note there are four answers for y^* and for each of them two answers for x^*. In order to find the unique collision point, one should evaluate the sum of distances of the collision points to the two foci for each of the eight points. The acceptable answer is the one which gives $2a$.

[1] B. J. Alder and T. E. Wainwright, J. Chem. Phys. **27**, 1208 (1957).

[2] B. J. Alder and T. E. Wainwright, Phys. Rev. **127**, 359 (1962); **1**, 18 (1970).

[3] M. P. Allen, D. Frenkel, and J. Talbot, Comput. Phys. Reports **9**, 301 (1989).

[4] P. G. de Gennes and J. Prost, *The Physics of Liquid Crystals*, 2nd ed. (Oxford University Press, Oxford, 1995).

[5] J. P. Hansen and I. R. McDonald, *Theory of Simple Liquids*, 2nd ed. (Academic Press, London, 1986).
[6] D. Frenkel, Mol. Phys. **60**, 1 (1987).
[7] C. DeMichele, R. Schilling, and F. Sciortino, Phys. Rev. Lett. **98**, 265702 (2007).
[8] P. Pfleiderer, K. Milinkovic, and T. Schilling, Euro. Phys. Lett. **84**, 16003 (2008).
[9] J. C. Armas-Perez and J. Quintana-H, Phys. Rev. E **83**, 051709 (2011).
[10] M. Doi, I. Yamamoto, and F. Kano, J. Phys. Soc. Jpn. **53**, 3000 (1984).
[11] M. Fixman, Phys. Rev. Lett. **54**, 337 (1985); **55**, 2429 (1985).
[12] Y. G. Tao, W. K. den Otter, J. K. G. Dehont, and W. J. Briels, J. Chem. Phys. **124**, 134906 (2006).
[13] M. Huthmann, T. Aspelmeier, and A. Zippelius, Phys. Rev. E **60**, 654 (1999).
[14] M. J. Green, R. A. Brown, and R. C. Armstrong, J. Chem. Phys. **126**, 034903 (2007).
[15] J. J. Magda, H. T. Davis, and M. Tirrell, J. Chem. Phys. **104**, 6755 (1996).
[16] H. H. Wensink and R. L. C. Vink, J. Phys.: Condensed Matter **19**, 466109 (2007).
[17] A. Chrzanowska, Acta. Phys. Pol. B **36**, 3163 (2005).
[18] M. Otto, T. Aspelmeier, and A. Zippelius, J. Chem. Phys. **124**, 154907 (2006).
[19] D. Frenkel, B. M. Mulder, and J. P. McTague, Phys. Rev. Lett. **52**, 287 (1984).
[20] J. W. Perram, M. S. Wertheim, J. L. Lebowitz, and G. O. Williams, Chem. Phys. Lett. **105**, 277 (1984).
[21] D. Frenkel and B. M. Mulder, Mol. Phys. **55**, 1171 (1985).
[22] M. P. Allen and D. Frenkel, Phys. Rev. Lett. **58**, 1748 (1987).
[23] M. P. Allen, Phys. Rev. Lett. **65**, 2881 (1990).
[24] M. Letz, R. Schilling, and A. Latz, Phys. Rev. E **62**, 5173 (2000).
[25] Th. Theenhaus, M. P. Allen, M. Letz, A. Latz, and R. Schilling, Eur. Phys. J. E **8**, 269 (2002).
[26] J. Vieillard-Baron, J. Chem. Phys. **56**, 4729 (1972).
[27] T. Boublik, Mol. Phys. **29**, 421 (1975).
[28] D. A. Ward and F. Lalo, Mol. Phys. **63**, 623 (1988).
[29] J. A. Cuesta, C. F. Tejero, and M. Baus, Phys. Rev. A **39**, 6498 (1989).
[30] K. J. Strandburg, Rev. Mod. Phys. **60**, 161 (1988).
[31] P. G. Ferreira, A. Perera, M. Moreau, and M. M. T. da Gama, J. Chem. Phys. **95**, 7591 (1991).
[32] J. A. Cuesta and D. Frenkel, Phys. Rev. A **42**, 2126 (1990).
[33] M. Moradi and R. Khordad, J. Chem. Phys. **125**, 214504 (2006).
[34] D. Frenkel and J. F. Maguire, Phys. Rev. Lett. **47**, 1025 (1981); Mol. Phys. **49**, 503 (1983).
[35] J. J. Magda, H. T. Davis, and M. Tirrell, J. Chem. Phys. **85**, 6674 (1986).
[36] C. Renner, H. Lowen, and J. L. Barrat, Phys. Rev. E **52**, 5091 (1995).
[37] A. Mukôyama and Y. Yoshimura, J. Phys. A: Math. Gen. **34**, 4053 (2001).
[38] A. Chrzanowska and H. Ehrentraut, Phys. Rev. E **66**, 012201 (2002).
[39] M. Jiménez-Ruiz, A. Criado, F. J. Bermejo, G. J. Cuello, F. R. Trouw, R. Fernández-Perea, H Löwen, C. Cabrillo, and H. E. Fischer, J. Phys.: Condens. Matter **14**, 1509 (2002).
[40] A. Mukôyama and Y. Yoshimura, Mol. Simul. **21**, 367 (1999).
[41] Y. Kantor and M. Kardar, Phys. Rev. E **79**, 041109 (2009).
[42] P. Gurin and S. Varga, Phys. Rev. E **83**, 061710 (2011).
[43] M. E. Foulaadvand and M. Yarifard, Eur. Phys. J. E **34**, 41 (2011).
[44] Y. Han, A. M. Alsayed, M. Nobili, J. Zhang, T. C. Lubensky, and A. G. Yodh, Science **314**, 626 (2006).
[45] A. Donev, S. Torquato, and F. H. Stillinger, J. Comp. Phys. **202**, 737 (2005).
[46] A. Donev, S. Torquato, and F. H. Stillinger, J. Comp. Phys. **202**, 765 (2005).
[47] K. Raghavan, Molec. Phys. **84**, 345 (1995).
[48] K. M. Sando and D. W. Rebertus, J. Chem. Phys. **67**, 2585 (1977).
[49] J. Talbot, M. P. Allen, G. T. Evans, D. Frenkel, and D. Kivelson, Phys. Rev. A **39**, 4330 (1989).
[50] P. Bereolos, J. Talbot, M. P. Allen, and G. T. Evans, J. Chem. Phys. **99**, 6087 (1993).
[51] X. Zheng and P. Palffy-Muhoray, Phys. Rev. E **75**, 061709 (2007).
[52] T. M. Truskett, S. Torquato, S. Sastry, P. G. Debenedetti, and F. H. Stillinger, Phys. Rev. E **58**, 3083 (1998).
[53] A. Jaster, Phys. Rev. E **59**, 2594 (1999).
[54] A. Donev, R. Connelly, F. H. Stillinger, and S. Torquato, Phys. Rev. E **75**, 051304 (2007).
[55] Murray Spiegel, *Schaums Mathematical Handbook of Formulas and Tables*, 2nd ed. (McGraw-Hill, New York, 1998).